analytical chemistry

Article

Cite This: *Anal. Chem.* 2020, 92, 1033−1040

pubs.acs.org/ac

Application of Biofunctionalized Magnetic Nanoparticles Based-Sensing in Abused Drugs Diagnostics

Serdar Sanli,[†] Faezeh Ghorbani-Zamani,[†] Hichem Moulahoum,[†] Zinar Pinar Gumus,[‡] Hakan Coskunol,[§] Dilek Odaci Demirkol,[†] and Suna Timur*[,†,‡]

[†]Department of Biochemistry, Faculty of Science, Ege University, 35100-Bornova, Izmir, Turkey

[‡]Central Research Test and Analysis Laboratory Application and Research Center, Ege University, 35100-Bornova, Izmir, Turkey

[§]Ege University, Faculty of Medicine, 35100-Bornova, Izmir, Turkey

Supporting Information

ABSTRACT: Real-time detection of substance use is an approach of high interest leading to the optimization of behavioral interventions and drug abuse intervention. The current methods in use suffer many limitations and need high logistical and laboratory requirements. Biosensors have shown a great potential in overcoming these limitations. In the present study, the electrochemical biosensor composed of a screen-printed electrode (SPE) was designed for the detection of synthetic cannabinoid (SC). Antibody-immobilized magnetic nanoparticles were also used to create a surface on the transducer with magnetic interactions in order to detect JWH-073 as a SC model. The use of immobilized magnetic nanoparticles to create working surfaces makes the electrode a reusable SPE which can be reutilized after the cleansing. To examine and observe any possible changes on the surface due to its interaction with the analyte, different electrochemical techniques such as differential pulse voltammetry, cyclic voltammetry, and electrochemical impedance spectrometry were applied. Based on the obtained results, the linearity of the biosensor was found between 5 and 400 ng/mL, and the detection limit was calculated as 22 ng/mL (n = 6) using the 3 Sb/m formula. The biosensor functionality was studied in the presence of some related interferents that showed lower responses than JWH-073, thus demonstrating the good selectivity of the prepared biosensor. Finally, the sensory platform was used to test synthetic urine sample, and the results were compared with obtained results from liquid chromatography quadrupole time-of-flight mass spectrometry (LC-QTOF/MS), which showed that the proposed method could be utilized to identify abuse drugs.

Statistics have shown a worldwide growth increase in abuse drugs, where more than 5% of the adult population have used some type of drugs over the past eight years.[1] Among the various types of drugs, cannabis is considered as one of the oldest abuse drugs preferred by 183 million of the global users compared to 35 million for opioids and 17 million users for cocaine during the past years.[2] Significant growth in cannabis consumption has had a huge impact on the synthetic cannabinoids (SCs) markets. SCs are one of the main chemical groups of the new psychoactive substances (NPSs) which are marketed as natural herbal mixtures under brand names such as Spice, Spice Gold, Spice Diamond, Arctic Spice, Silver, Aroma, K2, Genie, and Scene or Dream.[3] NPSs can be newly human-made designed compounds or old research chemicals, nutrition substances, and abandoned medications with similar effects of illegal drugs like cocaine, heroin, (+)-lysergide (LSD), ecstasy (MDMA), and methamphetamine.[4] Among the different types of NPSs, SCs showed a significant potential to replace cannabis by binding to the cannabinoid receptors and simulate the desired effects usually obtained from (−) transΔ^9-tetrahydrocannabinol (THC).[5,6] JWH-018 was the first detected SC that was blended with herbal smoking mixtures in 2008.[7] Low cost, easy access, and nonrecognizability of SCs in conventional urine toxicology screens made these compounds more preferable compared to other abuse drugs.[8,9] SCs consumptions have brought some critical health problems such as tachycardia, psychosis, agitation, anxiety, breathing difficulties, seizures, acute kidney injuries, brain structure damages, and lack of functionality.[6,10−13] Nonetheless, some aspects like cost efficient productions and capability to easily mimic the THC effects lead the SCs manufacturers to further widening the chemicals diversities creating many new versions.[14] The profitability of such SCs made the manufactures compete to produce many new versions that are hard to identify and unable to be detected.[4,5,15]

Traditional methods that usually rely on self-reporting or urine screening have some obvious limitations. The inability to

Received: September 3, 2019
Accepted: December 4, 2019
Published: December 4, 2019

DOI: 10.1021/acs.analchem.9b04025
Anal. Chem. 2020, 92, 1033−1040

measure patterns and frequencies of use and the failure of some respondents to disclose use and time of consumption are some of the limitations faced during screening. To avoid such scenarios, the use of biosensing devices and specific biosensors for drug use assessment and identification has received increasing interest.

Despite the acceptable costs and good performance of the electrochemical sensors for routine controls in the field, there are important obstacles faced during the regeneration of the sensing surface. The electrode surface recovery and reconstruction after binding to the tested elements are critical factors limiting the applications of sensors and biosensors.[16] Among the various options, magnetic nanoparticles (MNPs) are able to form a disposable and biocompatible recognition surface due to their magnetic behaviors. They seem to be a good and practical candidate to apply in biosensor structures. A well-positioned external neodymium magnet on the backside of the screen-printed electrodes (SPEs) can create a MNP layer on the transducers. The large surface area of MNPs increases analyte detection as well as enhances the biosensor response. In addition, the immobilization of biomolecule analytes on the MNPs helps to separate them from impurities and reduces the matrix effect under a magnetic field.[17]

MNPs can be easily synthesized by different methods such as sol−gel,[18] hydrothermal,[19] thermal decomposition,[20] normal or inverse micelle, and coprecipitation.[21] MNPs functionalization can be done by applying suitable materials like silica, polymers, or antibodies to increase the biocompatibility or functional behavior.[16] These multifunctional properties make MNPs favorable to use in various research areas like cellular labeling, drug delivery, MRI, hyperthermia, immunoassay, biosensors, and tissue repair.[17,22−25]

In the current paper, we propose a new SC detection method using data obtained from MNPs-based biosensor. In addition to the ferromagnetic features of iron oxide nanoparticles, other advantages such as easy preparation, low cost, large active surface area, and their noncytotoxic behaviors makes them a good tool for bioanalytical application.[26] One of the most outstanding features of MNPs is the possibility to concentrate the analyte before the detection step. Modified nanoparticles that carry the receptor units can be mixed easily with the analyte solution even at high concentrations and are able to interact selectively with the specific target. This type of MNPs-based biosensor can be simply reused by applying an external magnet which agglomerates and separates nanoparticles from the solution. In here, iron oxide MNPs were synthesized by a previously reported coprecipitation method[27,28] and modified with tetraethyl orthosilicate and (3-Aminopropyl)triethoxysilane (TEOS and APTES) to introduce amino functional groups on the surface and prevent integration of MNPs. MNP-K2 (MNPs covered with anti-K2 antibodies as biodetector components) were immobilized on the working electrode of the screen-printed electrode (SPE) via the help of external neodymium magnet (SPE/MNP-K2). A SPE/MNP-K2 sensing platform was used to detect JWH-073 (4-butanoic acid metabolite) as a SC model. Surface formation and analyte binding were followed via electrochemical techniques such as differential pulse (DPV), cyclic voltammetry (CV), and electrochemical impedance spectroscopy (EIS). Our empirical analysis showed the threshold of the parameters used to diagnose SC use and showed that the proposed method could be used to identify other abuse drugs. Moreover, single-drop sensing represents many advantages due to rapid preparation, fast measurement capability, low cost, and good analytical performance. All these advantages make this new SPE-based biosensor a potential candidate for on-field forensic applications.

EXPERIMENTAL SECTION

Materials. JWH-073 (4-butanoic acid metabolite), cocaine (COC), methamphetamine (METH), and benzoylecgonine (BE) were purchased from Cerilliant Corp (Round Rock, TX, USA). Tetrahydrocannabinol (THC) and monoclonal anti-K2 were supplied by THC Pharm (Biochem.thc-pharm, Germany) and Arista Biological (St. Allentown PA, 18101), respectively. Tetraethyl orthosilicate and (3-aminopropyl)triethoxysilane were supplied by Sigma (St. Louis, MO, USA), whereas the other chemical reagents were supplied by Sigma (St. Louis, MO, USA).

All chemicals used were of analytical grade. Synthetic urine was prepared according to previously described work and given in the Supporting Information (Table ST 1).[14] Milli-Q water was used in all solutions as a solvent.

Instrumentation. PalmSens potentiostat (Palm Instruments, Houten, Netherlands) driven by PC trace 5.3 software was used for differential pulse voltammetry (DPV) and cyclic voltammetry (CV). Electrochemical impedance spectroscopy (EIS) was studied by a CHI 6005 C electrochemical analyzer (CH Instruments Incorporated, Austin, TX, USA) to characterize SPE surface. The ceramic screen-printed SPE three-electrode system consists of Ag/AgCl reference electrode and two carbon electrodes as working and counter electrodes. The commercially available SPE (Dropsense DRP110) was purchased from Dropsense (Asturias, Spain) and used for all electrochemical measurements. Neodymium magnets were purchased from Megahand Information Technologies (Menemen, Izmir) to create magnetic interactions between the working electrode surface and MNP-K2. The electrochemical features of SPEs surfaces were studied by CV and EIS techniques (frequency range from 0.03 Hz to 10 kHz at +0.18 V) in the presence of HCF ($[Fe(CN)_6]^{(3-/4-)}$ as a water-soluble redox mediator. Analytical performance of a prepared SPE/MNP-K2 sensing platform was evaluated with DPV technique.

MNP and TEOS-APTES covered MNP samples were examined with transmission electron microscopy (TEM) for functional coating visualization. JEM-2100F microscope (JEOL, Tokyo, Japan) was used to capture the images of MNP samples after the drying process. Scanning electron microscopy (SEM) was used to obtain supporting images of analyte recognition. Samples were sputtered by 5 nm Au−Pd by using a Leica EM ACE600 model high vacuum sputter coater (Wetzlar, Germany), and images were taken by Thermo Fischer Scientific Apreo S LoVac model (Oregon, USA) equipped with a secondary electron detector operating at 8.0 and 10 kV. AFM images of all SPE samples before and after modification (SPE/MNP-K2/JWH-073) were monitored by Nanosurf Easyscan 2 atomic force microscopy system driven by Nanosurf Easyscan 2 Software. Three dimension AFM images were also processed with Gwyddion 2.39 software.

Chromatographic separation was performed by Agilent HPLC 1260 Infinity system. Mass analysis was studied by Agilent 6550 iFunnel high resolution accurate-mass Q-TOF/MS, equipped with Agilent dual jet stream electrospray ionization (Dual AJS ESI). Interface operating in a positive ion mode was used for the confirmation analysis of JWH-073

DOI: 10.1021/acs.analchem.9b04025
Anal. Chem. 2020, 92, 1033−1040

(Agilent Technologies, Santa Clara, CA, USA). Instrumental conditions were set the same as a previous work for chromatographic and mass analyses.[14]

MNP Synthesis and Modification. Modified Fe_3O_4 metallic nanoparticles were synthesized by the coprecipitation method under mild reaction conditions.[27,28] The solution of $FeCl_3$ (2.0 M) and $FeCl_2$ (1.0 M) was prepared under a nitrogen gas flow at 80 °C, while the solution was stirred vigorously. A NH_4OH solution (25 wt %) was added into the solution dropwise until the formation of black sediments stopped. To remove any possible impurities and unreacted reagents, MNPs precipitates were washed first with ethanol and then water. The obtained MNPs were dried at 80 °C for 8 h and stored at room temperature. In order to modify and introduce amino functional groups on MNPs surface, Stöber's functionalization procedure was applied.[29] For this purpose, MNPs (200 mg) were dispersed in ethanol/deionized water (100 mL, 8:2 (v:v)) and ammonia solution (2.5 mL). After stirring the mixture in the ultrasonic bath for 15 min, TEOS (5.0 mL) was added, and the solution was incubated for 12 h. Modified MNPs were washed with methanol several times to remove unreacted TEOS. All washing steps were done by the magnetic decantation method (Figure S2). TEOS-coated MNPs were redispersed in methanol (100 mL) and sonicated for 15 min. After sonication, APTES solution (5.0 mL) was added under vigorous stirring to obtain amino-functionalized MNP surfaces. To visualize and characterize the final fictionalized MNPs' surfaces, TEM was used.

Surface Modification, Electrochemical Characterization, and Measurements. Synthesized MNP-TEOS-APTES (5.0 mg) were dispersed in a phosphate buffered saline solution (500 μL, 50 mM, pH 7.4) under stirring. In order to prevent nanoparticles aggregation, the reaction was put in ultrasonic bath. The stock monoclonal anti-K2 (20 μL) was diluted 50 times in 2-[morpholino]ethanesulfonic acid) (MES) buffer (50 mM, pH 6.0). Then, the reaction was followed by the addition of N-(3-(dimethylamino)propyl)-N′-ethylcarbodiimide (EDC) (20 mg) and N-hydroxysuccinimide (NHS) (5.0 mg) to the diluted anti-K2 solution. After incubation for 15 min at room temperature, MNP-TEOS-APTES (500 μL) was added to EDC/NHS/anti-K2 mixture. The mixture was shaken for 2 h at 250 rpm. The obtained anti-K2-modified MNPs were washed with methanol several times to remove unreacted antibodies and labeled MNP-K2. MNP-K2 was redispersed in a phosphate buffer solution (500 μL of 50 mM, pH 7.4) under stirring conditions (Scheme 1A). For further steps, SPE surfaces were cleansed by soaking the electrodes in a H_2SO_4 solution (100 μL of 0.1 M).

The cyclic voltammetry (CV) technique was used to apply extreme anodic and cathodic potentials to remove impurities from the surface (−2.0 V to +2.0 V). After the cleaning procedure, SPE was rinsed by Milli-Q water. MNP-K2 (10 μL) in a phosphate buffer (50 mM, pH 7.4) was poured on SPE. A neodymium magnet was placed in the center backside of the SPEs working electrode. MNP-K2 was collected on the working electrode surface (SPE/MNP-K2) via magnetic interaction (Scheme 1B). Analytical performance and electrochemical characterization of MNP-K2-coated electrodes were studied by 100 μL of fresh prepared water-soluble redox probe (5.0 mM HCF in 0.1 M KCl). The DPV technique was used to visualize the signal responses with a potential range from −0.4 to +0.8 V. It was shown that DPV signals decreased after target analyte (JWH-073) binding to SPE/MNP-K2 surfaces. This

Scheme 1. (A) Modification of TEOS- and APTES-Coated MNPs with Monoclonal Anti-K2 Antibody by EDC/NHS chemistry. (B) Obtaining SPE/MNP-K2 Surface as Capturing of MNP-K2 on Working Electrode Surface by Magnetic Interactions. (C) Target Model SC Analyte (JWH-073) by SPE/MNP-K2 Surface Decreasing the DPV Signal

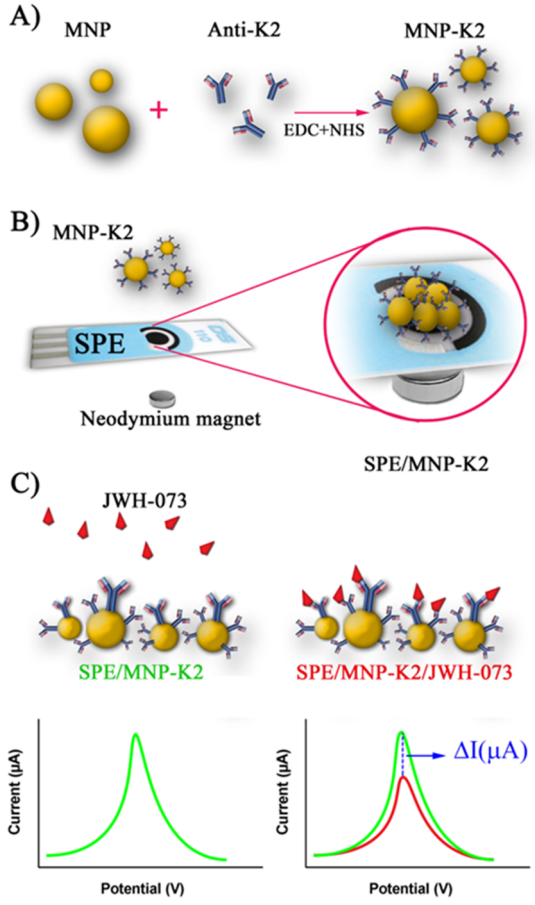

can be possibly due to JWH-073 electron transfer prevention through SPE/MNP-K2 (Scheme 1C). The increasing amount of the analyte causes significant DPV signals loss. The biosensor responses were calculated by using the difference in DPV signals before and after the addition of analytes which gives the difference between current values (ΔμA). Calibration curves of JWH-073−4-butanoic acid metabolite were obtained from different standard concentrations (5.0, 25, 50, 100, 200, 400 ng/mL) defined by $y = 0.035x + 1.561$ (R^2=0.998) equation.

Repeatability and Reproducibility of Biosensor. In order to confirm the repeatability of the SPE/MNP-K2 biosensor, repeated testing was performed on the same SPE. The unit was prepared as described above, and after testing and taking measurement, the biosensor was detached from the magnet. After washing the SPE, a fresh MNP-K2 solution was fixed again using a neodymium magnet. JWH-073 solution was added, and measurements were made. This procedure was repeated 10 times (n = 10).

For the reproducibility of the biosensor performance, different SPEs (n = 10) were taken and used for our analyte detection. Each SPE was tested for repeatability again as mentioned earlier. Results were calculated and statistically analyzed.

DOI: 10.1021/acs.analchem.9b04025
Anal. Chem. 2020, 92, 1033−1040

Confirmation of Biosensor with LC-QTOF/MS. For the confirmation analysis, synthetic urine samples were spiked with JWH-073 and then injected to the LC-QTOF/MS system. A calibration curve (50−1000 ng/mL) of JWH-073 was prepared in methanol from 1000 ng/mL of stock solution. The equation obtained for the calibration curve for JWH-073 is $y = 8238x + 56165$ with a correlation coefficient $R^2 = 0.9995$. An extracted ion chromatogram (EIC) of a spiked synthetic urine sample is shown in Figure S1 according to m/z 344.

Statistical Analysis. The selectivity of the biosensor, repeatability, and reproducibility were statistically analyzed using a one-way ANOVA test between the different groups (GraphPad Prizm Ver.8, San Diego). $p < 0.05$ was considered as statistically significant.

DISCUSSION

In the current study, a MNP/antibody conjugate-based SC biosensor platform was constructed, and JWH-073 was used as a SC model. MNPs were synthesized by the coprecipitation method in the presence of $FeCl_2$ and $FeCl_3$ salts as described in the Experimental Section. After functionalization of MNPs surfaces with TEOS and APTES, TEM was used to visualize magnetic cores and amino-functionalized shells. As is shown in Figure 1A and B, MNP cores are approximately 15−20 nm,

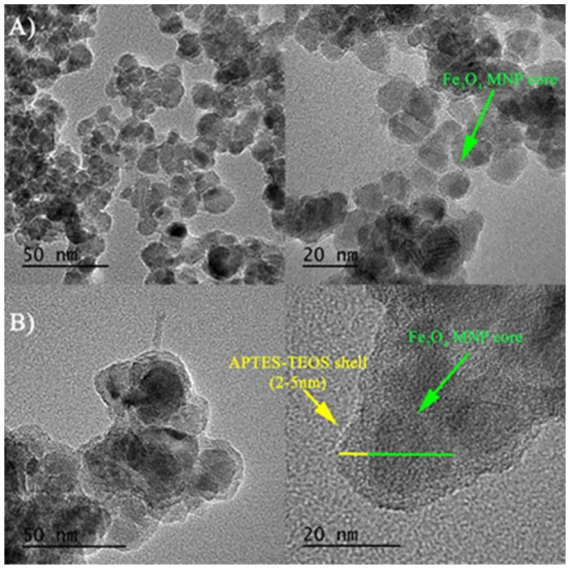

Figure 1. Transmission electron microscopy (TEM) images of (A) pristine MNPs and (B) core−shell structure of TEOS-APTES modified MNPSs with different magnifications.

whereas the shell structures can be easily seen with 2.0−5.0 nm thicknesses. Owing to EDC/NHS specific chemical features, covalent bonds were formed as a result of the carboxyl group of anti-K2 reactions with the amino group of MNPs. However, MNP-K2 was immobilized on the working electrode surface by magnetic interactions.

CV and EIS measurements and AFM and SEM images were taken stepwise for each bare SPE, MNP-K2 immobilized SPE, and JWH-073-captured SPE/MNP-K2. As can be seen in Figure 2A, after immobilization of MNP-K2 on the SPE working electrode's surface, peak potentials were increased as a result of the amine groups presence on the MNPs surface. Similar results were also observed in our previous works in which polyamidoamine (PAMAM) dendrimers were used to

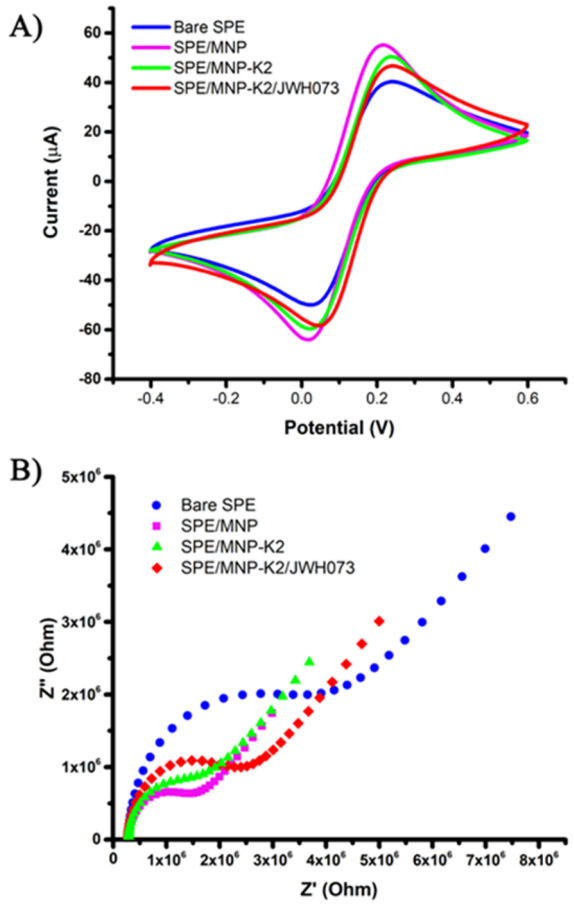

Figure 2. (A) CV and (B) Nyquist diagrams of Bare SPE, SPE/MNP, SPE/MNP-K2, and SPE/MNP-K2/JWH-073 surfaces [JWH-073 100 ng/mL]. [Randle's equivalent circuit was used to fit Nyquist plots, and these were shown in graphs]. [All measurements were carried out in 50 mM, pH 7.4 sodium phosphate buffer containing 5.0 mM $[Fe(CN)6]^{3-/4-}$ and 0.1 M KCl].

modify the electrode surfaces.[30,31] We previously showed PAMAM-positively charged amine groups have interacted with redox probes to increase peak potentials.[30,31] On the contrary, when JWH-073 was binding to SPE/MNP-K2, peak currents decreased due to electron transfer prevention between the redox probe and MNP-K2. Anodic peak currents were recorded as 47.079 μA for bare SPE, 66.126 μA for SPE/MNP, 60.294 μA for SPE/MNP-K2, and 55.081 μA for SPE/MNP-K2/JWH-073. On the other hand, cathodic peak currents were found to be at 51.251 μA for bare SPE, 67.523 μA for SPE/MNP, 61.901 μA for SPE/MNP-K2, and 60.321 μA for SPE/MNP-K2/JWH-073. Peak to peak separations were observed as 0.202 V for bare SPE, 0.189 V for SPE/MNP, 0.208 V for SPE/MNP-K2, and 0.185 V for SPE/MNP-K2/JWH-073. EIS analysis was another electrochemical method used to verify successful surface modifications. Randle's equivalent circuit which shows the resistance of electron transfer as a semicircle in Nyquist plots was used to fit raw EIS data. The design of Randle's equivalent circuit contains solution resistance (R_s), Warburg impedance (Z_w) resulting from diffusion of the $[Fe(CN)_6]^{(3-/4-)}$ redox probe, double layer capacitance (C_{dl}), and charge transfer resistance (R_{ct}). As was exhibited in Figure 2B, the R_{ct} value of the Nyquist plot dramatically decreased from 2938 to 1181 Ω by magnetic immobilization of MNP-K2 on bare SPE and

DOI: 10.1021/acs.analchem.9b04025
Anal. Chem. 2020, 92, 1033−1040

increased to 1852 Ω after capturing JWH-073 by anti-K2. This decreasing R_{ct} indicates an increase in the electron transfer procedure caused by the interaction between amine groups and the redox probe. In contrast, increasing R_{ct} can be explained by the prevention of interfacial charge transfer which decreases conductivity. Also, the nonmodified MNPs' R_{ct} value (1075 Ω) was found to be lower than the MNP-K2 surface. This conductivity difference can be explained as the anti-K2-coated MNP surface preventing interaction between the redox probe and amine groups. It is assumed that interfacial charge transfer was decreased by this coating effect.

In order to consider any changes on the electrode surface morphology, AFM images were taken. As illustrated in Figure 3, the surface roughness observed was estimated as 36.63 nm

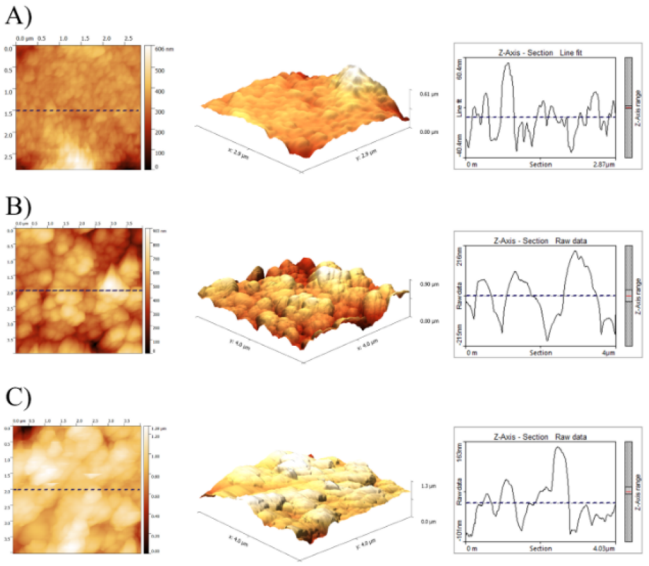

Figure 3. 2D and 3D AFM images and cross sections of (A) Bare SPE, (B) SPE/MNP-K2, and (C) SPE/MNP-K2/JWH-073.

for bare SPE, 74.02 nm for the SPE/MNP-K2-coated surface, and 89.99 nm for SPE/MNP-K2/JWH-073 by Nanosurf Easyscan 2 software. Increasing roughness values indicate successful modifications for each step. The surface morphology differences before and after analyte recognition were seen as filled with the voids in SEM images (Figure 4). To evaluate the analytical performance of our novel MNP-antibody-based JWH-073 biosensor, the DPV technique was applied to SPE in the presence of the same redox probe with CV and EIS. Different JWH-073 concentrations (5.0, 25, 50, 100, 200, 400 ng/mL in 10 mM sodium phosphate buffer, pH 7.4) were utilized during experiments (DPV calibration is presented in Figure S3). SPE could be used repeatedly after the cleaning process due to the noncovalent immobilization of MNP-K2 on the working electrode surface. After addition of JWH-073 with different concentrations to SPE/MNP-K2, DPV signals decreased significantly as shown in Figure 5A. JWH-073 detection has been done by measuring the difference in peak currents of SPE/MNP-K2 and SPE/MNP-K2/JWH-073. According to the obtained calibration curve, linearity was defined by the equation $y = 0.03482x + 1.5606$ ($R^2 = 0.998$) in the range of 5.0−400 ng/mL of JWH-073 (Figure 5B). Based on the obtained results, it can be concluded that a magnetic-antibody-based SPE/MNP-K2 sensor could be seen as a good candidate for JWH-073 analysis. Other analytical parameters

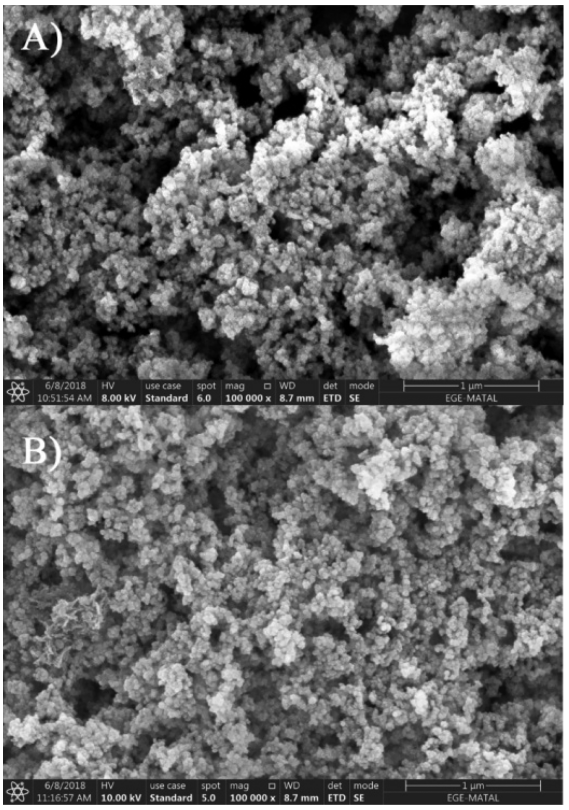

Figure 4. SEM images of (A) SPE/MNP-K2 and (B) SPE/MNP-K2/JWH-073.

such as repeatability and limit of detection (LOD) for SPE/MNP-K2 were also studied.

Repeatability was examined with 10 consecutive measurements, while ±SD and coefficient of variation (C.V.) were calculated as ±0.607 and 4.5% ([Sb/average] × 100), respectively. In addition, the reproducibility of the biosensor showed no significant difference between different SPE units ($p > 0.05$) (Figure 6A). The raw values of all the measurements ($n = 10$) obtained after DPV are included in the Supporting Information section (Table ST 2), while Figure 6A shows three representative electrodes.

The LOD was calculated as 22 ng/mL ($n = 6$) with the 3Sb/m formula. General analytical performance is summed in Table 1.

The concentration of a 100 ng/mL spiked synthetic urine sample was found to be 107.52 ng/mL with LC-QTOF/MS analysis. The same process was followed on the current biosensor for measuring the concentration of a synthetic urine sample. The concentration of the same sample was shown as 101.52 ± 4.77 ng/mL, thus confirming the successful performance of the designed biosensor. The raw data of the calibration and measurement with LC-QTOF/MS are included in the Supporting Information, Figure S4.

To evaluate the selectivity of JWH-073 biosensor platform, the performance of the biosensor was examined in the presence of some analyte-related possible interferents such as benzoylecgonine (BE), methamphetamine (METH), nicotine, and cotinine. For this purpose, 100 ng/mL of each interferent was added to the biosensor platform by following the same experimental conditions used to determine JWH-073. As a result, SPE/MNP-K2 did not show any significant feedbacks for selected analytes ($p > 0.05$) contrary to JWH-073 ($p <$

DOI: 10.1021/acs.analchem.9b04025
Anal. Chem. 2020, 92, 1033−1040

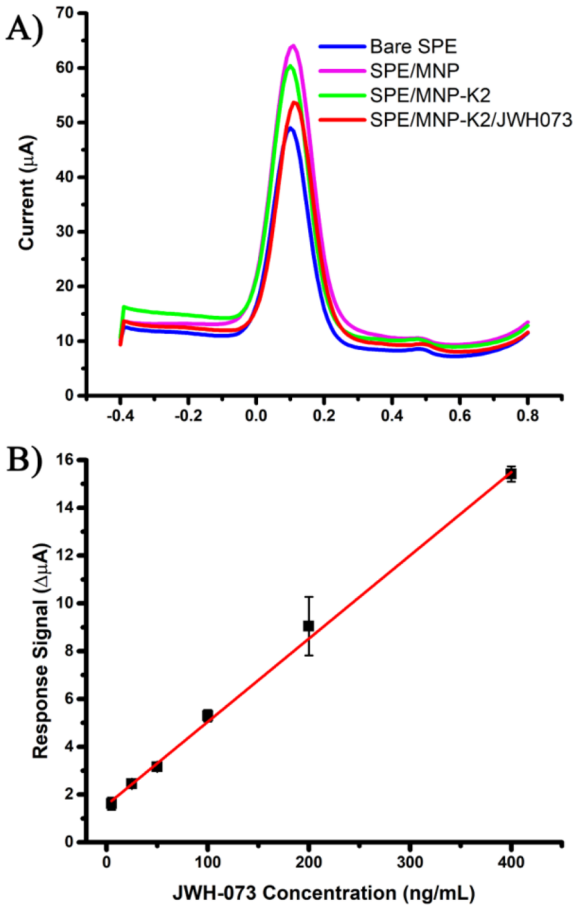

Figure 5. (A) DPV curves of Bare SPE, SPE/MNP, SPE/MNP-K2, and SPE/MNP-K2/JWH-073 surfaces [JWH-073; 100 ng/mL]. (B) Calibration curve of SPE/MNP-K2/JWH-073 obtained by DPV technique. [Measurements were carried out in 50 mM, pH 7.4 sodium phosphate buffer containing 5.0 mM $[Fe(CN)6]^{3-/4-}$ and 0.1 M KCl]. [Error bars shows ± S.D.].

0.001) (Figure 6B). The obtained results proved the selectivity of the designed SPE/MNP-K2 platform to JWH-073 as a SC model. Furthermore, a comparison between our biosensor and other sensors for synthetic cannabinoids detection was made and is summarized in Table 2.

One of the major difficulties seen in the abused drug sensing is the heaviness of the techniques and the length of the procedures. Many attempts such as ours to create portable biosensors for on-site detection have been made. For example, molecular imprinted polymers (MIPs) showed a lot of potential in this field. However, it has been shown that compared to SPE/MNP biosensors, the binding times of MIPs takes hours to achieve while the loading is considerably low. In the current study, the preparation of the biosensor takes around 15−30 min. This can be considered as a great development in the making of portable biosensors.

CONCLUSIONS

In this paper, the design and preparation of a novel MNPS-based SC biosensor was reported. According to our knowledge, it is the first time that anti-K2 antibodies were used to surround the amino functional MNPs surface to create a biofunctionalized MNP-K2 layer. The approach focused on the immobilization of anti-K2 antibodies on the SPE working electrode via a magnetic field created by neodymium magnet.

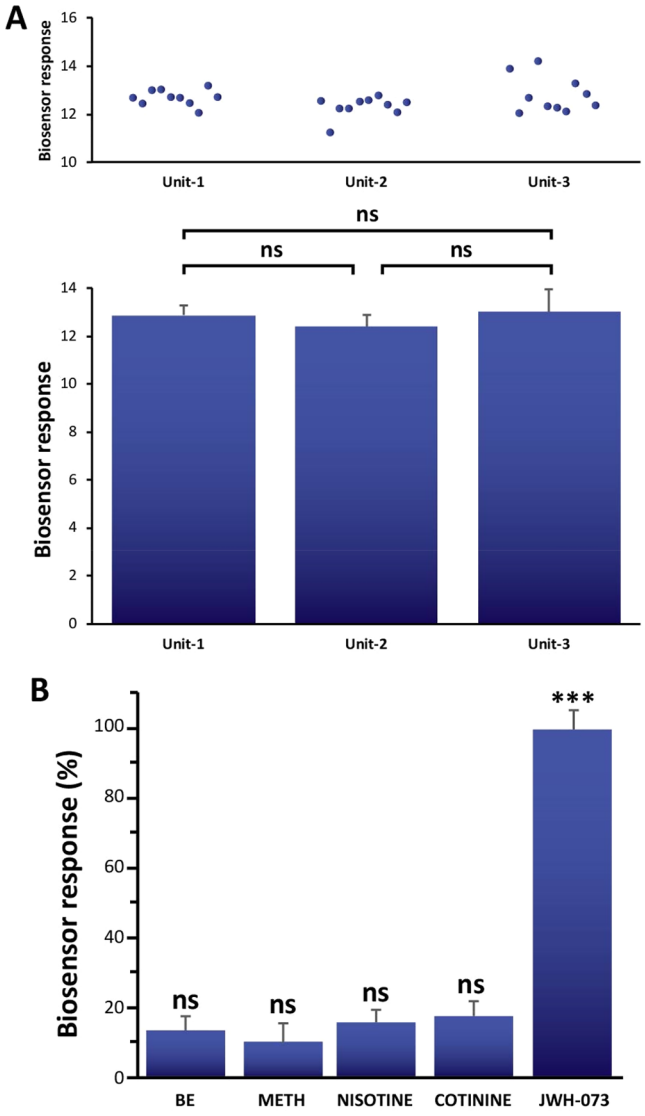

Figure 6. Biosensor performance. (A) Repeatability and reproducibility of the bisensor measured according to description in the Experimental Section. (Three representative results are demonstrated; raw data is included in Table ST 2, Supporting Information). (B) Response of the biosensor to some selected interferents (n = 10) (ns: nonsignificant, ***p < 0.001 vs SPE/MNP-K2).

Table 1. Some Analytical Properties of Designed MNP-K2/JWH-073 Sensor

Analytical properties	Values
Linear range [LOD, ng/mL]	5.0−400
Limit of detection [ng/mL]	22.0
Repeatability [±S.D.]	0.607
Coefficient of variation [%]	4.5

This novel biosensor platform was tested successfully on synthetic urine samples which included 100 ng/mL of JWH-073, and the results were compared with LC-QTOF/MS system. Verification results proved that the proposed biosensor has a great selectivity and sensitivity for JWH-073. Magnetic immobilization of antibodies on SPE presents many advantages like high affinity, rapid preparation, adaptable for portable biosensor designs, good selectivity, low chemical volumes use (from mL to μL), and SPEs reusability with easy cleaning

DOI: 10.1021/acs.analchem.9b04025
Anal. Chem. 2020, 92, 1033−1040

Table 2. Comparison of Other Reported Surface Materials for JWH-073 Sensors[a]

Analytical Methods/Techniques	Concentration range	Detection limit	Sample	Confirmation methods	ref
DPV	5−400 ng/mL	22 ng/mL	Synthetic urine	LC-QTOF/MS	This work
QCM mass variation	0.0005−1.0 ng/mL	0.45 pg/mL	Synthetic urine	LC- MS	32
DPV	25−500 ng/mL	31.87 ng/mL	Synthetic urine	LC-QTOF/MS	33
DPV	5−20 mg/L	50 μg/L	Synthetic saliva	GC-MS and LC-MS	34
DPV	5−400 ng/mL	22 ng/mL	Synthetic urine	LC-QTOF/MS	This work
MALDI-TOF MS	Not given	Not given	Herbal blends	GC-MS	35
GC-MS/MS	5−20 mg/g	Not given	Herbal blends	HPLC	36
LC-MS/MS	1−10 pg/mg	0.5 pg/mg	Hair	–	37
GC-MS	2.5−100 mg/L	0.5 mg/mL	Herbal blends	–	38
LC-MS	0.2−60 ng/mL	0.6 ng/mL	Urine	–	39
LC-MS/MS (Q-TOF)	Not given	Not given	Herbal blends	GC-MS	35
HPLC/MS/MS	67−244 ng/mL	4.3 ng/mL	Mice blood	–	40

[a]Quartz crystal microbalance (QCM), hyperbranched P(MMA-*co*-DMAEMA), methyl methacrylate (MMA), 2-(dimethylamino) ethyl methacrylate (DMAEMA), glassy carbon electrode (GCE), benzoylecgonine (BE), gold nanoparticles (AuNPs), paper microfluidic devices (μPADs), synthetic cannabinoid (SCs), molecular imprinted polymer (MIP), boron-doped diamond electrodes (BDD), screen-printed electrode (SPE), magnetic nanoparticles (MNPs), and matrix-assisted laser desorption ionization-time-of-flight mass spectrometry (MALDI-TOF MS).

procedures. Given the good analytical performance by changing the SC formula made this type of biosensor a practical device to recognize small amounts of synthetic abuse drugs.

■ ASSOCIATED CONTENT

Supporting Information

The Supporting Information is available free of charge at https://pubs.acs.org/doi/10.1021/acs.analchem.9b04025.

ST 1: Synthetic urine composition in units of g/L and mM. ST 2: Repeatability and reproducibility results obtained from 10 different biosensors with each biosensor reused 10 times. Figure S1: EIC for the urine sample. Figure S2: Magnetic decantation of MNPs. Figure S3: DPV calibration of the biosensor. Figure S4: Raw data of measurement and calibration of LC-QTOF/MS. (PDF)

■ AUTHOR INFORMATION

Corresponding Author

*E-mail: suna.timur@ege.edu.tr.

ORCID

Hichem Moulahoum: 0000-0003-3934-6415

Dilek Odaci Demirkol: 0000-0002-7954-1381

Suna Timur: 0000-0002-3129-8298

Author Contributions

The manuscript was written through equal contributions of all authors. All authors have given approval to the final version of the manuscript.

Notes

The authors declare no competing financial interest.

■ ACKNOWLEDGMENTS

This work was funded by Republic of Turkey, Ministry of Development (Project Grant No: 2016K121190). SEM and Chromatographic analyses were performed at EGE MATAL (Ege University/Izmir). Ege University, Aliye USTER Foundation is also acknowledged for the financial support.

■ REFERENCES

(1) United Nations Office on Drugs and Crime. Global Overview of Drug Demand and Supply. In *World Drug Report*; 2017; pp 1−66.

(2) United Nations Office on Drugs and Crime. Market Analysis of Plant-Based Drugs. In *World Drug Report*; 2017; pp 1−68.

(3) Fattore, L.; Fratta, W. *Front. Behav. Neurosci.* **2011**, *5*, 60.

(4) Wille, S. M. R.; Eliaerts, J.; Di Fazio, V.; Samyn, N.Challenges Concerning New Psychoactive Substance Detection in Oral Fluid. *Toxicologie Analytique et Clinique*, February 2017; pp 11−17.

(5) Marusich, J. A.; Wiley, J. L.; Lefever, T. W.; Patel, P. R.; Thomas, B. F. *Neuropharmacology* **2018**, *134*, 73−81.

(6) Duccio, P.; Fabrizio, S.; Laura, O. Synthetic Cannabinoids and Synthetic Cannabinoid-Induced Psychotic Disorders. In *The Complex Connection Between Cannabis and Schizophrenia*; Academic Press, 2018; pp 199−220.

(7) Piggee, C. *Anal. Chem.* **2009**, *81* (9), 3205−3207.

(8) Zawilska, J. B.; Andrzejczak, D. *Drug Alcohol Depend.* **2015**, *157*, 1−17.

(9) Cooper, Z. D.; Poklis, J. L.; Liu, F. *Neuropharmacology* **2018**, *134*, 92−100.

(10) Tait, R. J.; Caldicott, D.; Mountain, D.; Hill, S. L.; Lenton, S. *Clin. Toxicol.* **2016**, *54* (1), 1−13.

(11) Livny, A.; Cohen, K.; Tik, N.; Tsarfaty, G.; Rosca, P.; Weinstein, A. *Eur. Neuropsychopharmacol.* **2018**, *28* (9), 1047−1057.

(12) Deng, H.; Verrico, C. D.; Kosten, T. R.; Nielsen, D. A. *Psychiatry Res.* **2018**, *268*, 400−412.

(13) Mills, B.; Yepes, A.; Nugent, K. *Am. J. Med. Sci.* **2015**, *350*, 59−62.

(14) Sengel, T. Y.; Celik, E. G.; Aydogan, C.; Gumus, Z. P.; Ilktac, R.; Aydindogan, E.; Ciftci, M.; Aldemir, E.; Coskunol, H.; Timur, S.; et al. *ChemElectroChem* **2018**, *5* (9), 1253−1258.

(15) Langford, A. M.; Bolton, J. R. *J. Forensic Leg. Med.* **2018**, *59*, 36−38.

(16) Xu, Y.; Wang, E. *Electrochim. Acta* **2012**, *84*, 62−73.

(17) Xianyu, Y.; Wang, Q.; Chen, Y. *TrAC, Trends Anal. Chem.* **2018**, *106*, 213−224.

(18) Owens, G. J.; Singh, R. K.; Foroutan, F.; Alqaysi, M.; Han, C. M.; Mahapatra, C.; Kim, H. W.; Knowles, J. C. *Prog. Mater. Sci.* **2016**, *77*, 1−79.

(19) Attallah, O. A.; Girgis, E.; Abdel-Mottaleb, M. M. S. A. *J. Magn. Magn. Mater.* **2016**, *397*, 164−175.

(20) Jović Orsini, N.; Babić-Stojić, B.; Spasojević, V.; Calatayud, M. P.; Cvjetićanin, N.; Goya, G. F. *J. Magn. Magn. Mater.* **2018**, *449*, 286−296.

(21) Sharifi, I.; Shokrollahi, H.; Doroodmand, M. M.; Safi, R. *J. Magn. Magn. Mater.* **2012**, *324* (10), 1854−1861.

(22) Pérez-Herrero, E.; Fernández-Medarde, A. *Eur. J. Pharm. Biopharm.* **2015**, *93*, 52−79.

(23) Hedayatnasab, Z.; Abnisa, F.; Daud, W. M. A. W. *Mater. Des.* **2017**, *123*, 174−196.

DOI: 10.1021/acs.analchem.9b04025
Anal. Chem. 2020, 92, 1033−1040

(24) Razo, S. C.; Panferov, V. G.; Safenkova, I. V.; Varitsev, Y. A.; Zherdev, A. V.; Dzantiev, B. B. *Anal. Chim. Acta* **2018**, *1007*, 50−60.
(25) Clemons, T. D.; Kerr, R. H.; Joos, A. *Compr. Nanosci. Nanotechnol.* **2019**, 193−210.
(26) Neuberger, T.; Schöpf, B.; Hofmann, H.; Hofmann, M.; Von Rechenberg, B. *J. Magn. Magn. Mater.* **2005**, *293*, 483−496.
(27) Guldu, O. K.; Unak, P.; Medine, E. I.; Barlas, F. B.; Muftuler, F. Z. B.; Timur, S. *Int. J. Polym. Mater.* **2015**, *64* (5), 253−259.
(28) Petcharoen, K.; Sirivat, A. *Mater. Sci. Eng., B* **2012**, *177* (5), 421−427.
(29) Chen, M.; Qu, H.; Zhu, J.; Luo, Z.; Khasanov, A.; Kucknoor, A. S.; Haldolaarachchige, N.; Young, D. P.; Wei, S.; Guo, Z. *Polymer* **2012**, *53*, 4501−4511.
(30) Akin, M.; Yuksel, M.; Geyik, C.; Odaci, D.; Bluma, A.; Höpfner, T.; Beutel, S.; Scheper, T.; Timur, S. *Biotechnol. Prog.* **2010**, *26* (3), 896−906.
(31) Yuksel, M.; Akin, M.; Geyik, C.; Demirkol, D. O.; Ozdemir, C.; Bluma, A.; Höpfner, T.; Beutel, S.; Timur, S.; Scheper, T. *Biotechnol. Prog.* **2011**, *27* (2), 530−538.
(32) Battal, D.; Akgönüllü, S.; Yalcin, M. S.; Yavuz, H.; Denizli, A. *Biosens. Bioelectron.* **2018**, *111*, 10−17.
(33) Sengel, T. Y.; Celik, E. G.; Aydogan, C.; Gumus, Z. P.; Ilktac, R.; Aydindogan, E.; Ciftci, M.; Aldemir, E.; Coskunol, H.; Timur, S.; Yagci, Y. *ChemElectroChem* **2018**, *5* (9), 1253−1258.
(34) Dronova, M.; Smolianitski, E.; Lev, O. *Anal. Chem.* **2016**, *88* (8), 4487−4494.
(35) Gottardo, R.; Chiarini, A.; Dal Prà, I.; Seri, C.; Rimondo, C.; Serpelloni, G.; Armato, U.; Tagliaro, F. *J. Mass Spectrom.* **2012**, *47* (1), 141−146.
(36) Logan, B. K.; Reinhold, L. E.; Xu, A.; Diamond, F. X. *J. Forensic Sci.* **2012**, *57* (5), 1168−1180.
(37) Kim, J.; In, S.; Park, Y.; Park, M.; Kim, E.; Lee, S. *Anal. Bioanal. Chem.* **2013**, *405* (30), 9769−9778.
(38) Choi, H.; Heo, S.; Choe, S.; Yang, W.; Park, Y.; Kim, E.; Chung, H.; Lee, J. *Anal. Bioanal. Chem.* **2013**, *405* (12), 3937−3944.
(39) Sundstrom, M.; Pelander, A.; Angerer, V.; Hutter, M.; Kneisel, S.; Ojanpera, I. *Anal. Bioanal. Chem.* **2013**, *405* (26), 8463−8474.
(40) Poklis, J. L.; Amira, D.; Wise, L. E.; Wiebelhaus, J. M.; Haggerty, B. J.; Poklis, A. *Forensic Sci. Int.* **2012**, *220* (1−3), 91−96.

DOI: 10.1021/acs.analchem.9b04025
Anal. Chem. 2020, 92, 1033−1040